Effect of Respiratory Gating on Quantifying PET Images of Lung Cancer

Sadek A. Nehmeh, PhD[1]; Yusuf E. Erdi, DSc[1]; Clifton C. Ling, PhD[1]; Kenneth E. Rosenzweig, MD[2]; Heiko Schoder, MD[3]; Steve M. Larson, MD[3]; Homer A. Macapinlac, MD[4]; Olivia D. Squire, RN[3]; and John L. Humm, PhD[1]

[1]*Department of Medical Physics, Nuclear Medicine Service, Memorial Sloan-Kettering Cancer Center, New York, New York;*
[2]*Department of Radiation Oncology, Nuclear Medicine Service, Memorial Sloan-Kettering Cancer Center, New York, New York;*
[3]*Department of Radiology, Nuclear Medicine Service, Memorial Sloan-Kettering Cancer Center, New York, New York; and*
[4]*Department of Nuclear Medicine, The University of Texas, M.D. Anderson Cancer Center, Houston, Texas*

We have developed a new technique to gate lung ^{18}F-FDG PET images in synchronization with the respiratory motion to reduce smearing due to breathing and improve quantitation of ^{18}F-FDG uptake in lung lesions. **Methods:** A camera-based respiratory gating system, the real-time position management (RPM), is used to monitor the respiratory cycle. The RPM provides a trigger to the PET scanner to initiate the gating cycle. Each respiratory cycle is divided into discrete bins triggered at a defined amplitude or phase within the patient's breathing motion, into which PET data are acquired. The acquired data within the time bins correspond to different lesion positions within the breathing cycle. The study includes 5 patients with lung cancer. **Results:** Measurements of the lesions' volumes in the gated mode showed a reduction of up to 34% compared with that of the nongated measurement. This reduction in the lesion volume has been accompanied by an increase in the intensity in the ^{18}F-FDG signal per voxel. This finding has resulted in an improvement in measurement of the maximum standardized uptake value (SUV_{max}), which increased in 1 patient by as much as 159%. The total lesion glycolysis, defined as the product of the SUV_{max} and the lesion volume, was also measured in gated and nongated modes and showed a consistency between the 2 measurements. **Conclusion:** We have shown that image smearing can be reduced by gating ^{18}F-FDG PET images in synchronization with the respiratory motion. This technique allows a more accurate definition of the lesion volume and improves the quantitation specific activity of the tracer (in this case, ^{18}F-FDG), which are distorted because of the breathing motion.

Key Words: ^{18}F-FDG; respiratory gating; standard uptake value; total lesion glycolysis; lung cancer

J Nucl Med 2002; 43:876–881

Improvements in the accuracy of diagnostic imaging techniques can have an important impact in delineating malignant structures within the lung and monitoring tumor response to therapy. This is especially critical in radiotherapy, where the accurate definition of the tumor volume and position determines the radiation treatment fields and the volume of irradiated lung. CT is the most frequently used diagnostic technique to provide anatomic and morphologic information. However, CT has a lower sensitivity (68%) and specificity (61%) in lung compared with ^{18}F-FDG PET (87% and 91%, respectively) for detecting disease (*1*). ^{18}F-FDG PET, which takes advantage of the increase in the glucose uptake within lesions (*2*), can provide metabolic and physiologic information about lesions and is important for staging of the disease. ^{18}F-FDG PET has also been considered to be a useful tool to monitor the tumor response to treatment (*2*), through measurement of various semiquantification parameters—in particular, the standardized uptake value (SUV). A measured SUV of >2.5 (measured with a filtered backprojection reconstruction algorithm) is usually considered to indicate a higher probability for malignancy (*3*). The SUV measurement in combination with other parameters, such as the lesion site and the shape (*4*), is used to make the final assessment of the disease status. Another quantification parameter is the total lesion glycolysis (TLG) (*2*).

In lung cancer, these parameters may be distorted from their actual values because of respiration. Respiratory motion reduces image quality by reducing the target-to-background ratio (contrast), resulting in image blurring. Respiration may also result in overestimation of the lesion size. The consequence of these effects is a possible misidentification of the lesion. The number of counts acquired during a time *t*, whether the lesion is static or moving, is the same. Therefore, any increase in the apparent lesion size due to motion will decrease the activity concentration per pixel within the lesion (*5*), thereby reducing the lesion contrast. Consequently, the measured SUVs will underestimate the glucose concentration within the tumors. Therefore, a 2.5 cutoff threshold should not be correlated with malignancy in lung cancer, but a new SUV cutoff threshold must be investigated. The 2.5 cutoff threshold has been obtained

Received Aug. 10, 2001; revision accepted Feb. 21, 2002.
For correspondence or reprints contact: Sadek A. Nehmeh, PhD, Department of Medical Physics, Nuclear Medicine Service, Memorial Sloan-Kettering Cancer Center, 1275 York Ave., New York, NY 10021.
E-mail: nehmehs@mskcc.org

empirically from the evaluation of patients with lesions of different ^{18}F-FDG uptake in different sites and different positions in the lung. Therefore, the intrinsic FDG accumulation used to derive the SUV is smeared by lesion motion caused by respiration. This study removes the statistical uncertainties introduced by motion and suggests reevaluation of the SUV threshold for lung cancer. Because the degree of lesion motion is dependent on the location within the lung (i.e., proximity to the diaphragm), the error associated with activity estimation is site dependent. Hence, an improvement toward reducing the respiratory motion artifacts is needed to improve the level of confidence in the PET measured quantification parameters. These motion artifacts can be compensated by acquiring PET data into discrete bins within each respiratory cycle, with the first bin triggered at a user predefined position within the breathing cycle (*5*). The number of bins is optimized with the patient's breathing cycle to minimize the lesion motion within a single time interval. Phantom studies showed a major dependence on the reduction in the smearing effect on the bin size for defined lesion size and motion amplitude (*5*). Those studies also showed that the reduction in the motion artifacts is a function of the amplitude and the lesion size for a defined bin size. In this article, we present clinical data showing the potential benefits of respiratory gating in PET imaging. Five patients were considered for this study, all with lung cancer.

MATERIALS AND METHODS

PET Scanner

Data were acquired using an Advance PET camera (General Electric Medical Systems, Waukesha, WI), a whole-body scanner with a transaxial field of view (FOV) of 55 cm with 14.75 cm along the axial direction. The scanner contains retractable septa and can be used in 2 dimensions (septa extended) for high-resolution imaging (2-dimensional mode used in this study). The image resolution is 4.2-mm full width at half maximum.

Gating System

Our gating tool is the Real-Time Position Management (RPM) Respiratory Gating System (Varian Medical Systems, Palo Alto, CA) designed initially for radiotherapy gating. The RPM tracks the respiratory cycle by monitoring the chest motion of the patient through the use of 2 passive reflective markers rigidly mounted on a lightweight plastic block. The block is stabilized on the patient's abdomen, and its motion is monitored and tracked using an infrared video camera mounted on the PET table (Fig. 1). By simultaneous tracking of the 2 markers, the system maintains calibration of the vertical component of the motion. The motion of the block is displayed by a graphic interface on the screen of the RPM workstation. A training session is performed first, where a prototype of the breathing motion is defined by the RPM. This is done to determine whether the patient's breathing cycles are regular, compared with the prototype, during the scan. The user is then able to generate a trigger signal (output by the RPM) at a selected phase or amplitude within the breathing cycle. The trigger will then be generated by the RPM every time the phase (amplitude) of the breathing cycle is regular at the defined position compared with the prototype. More details about the RPM system can be found in Kubo et al. (*6*).

Data Acquisition

PET data are acquired into discrete bins in synchronization with the breathing cycle. The number of time bins and the duration of each bin are set before obtaining the scan on the PET console. The trigger generated by the RPM is used to flag the first bin in the PET data acquisition cycle. As a result, for each transaxial position along the lesion, multiple images (each corresponding to a 1-time bin) are generated. More details can be found in Nehmeh et al. (*5*). Because of the short time interval of each bin (300–500 ms), the lesion motion is expected to be negligible within each of them. Hence, the images reconstructed within each time bin exhibit a reduction in the motion smearing.

Patients

Five patients were considered prospectively in this study (Table 1). Each of these patients was studied with static and gated PET (10 bins) techniques. All patients had already undergone CT sim-

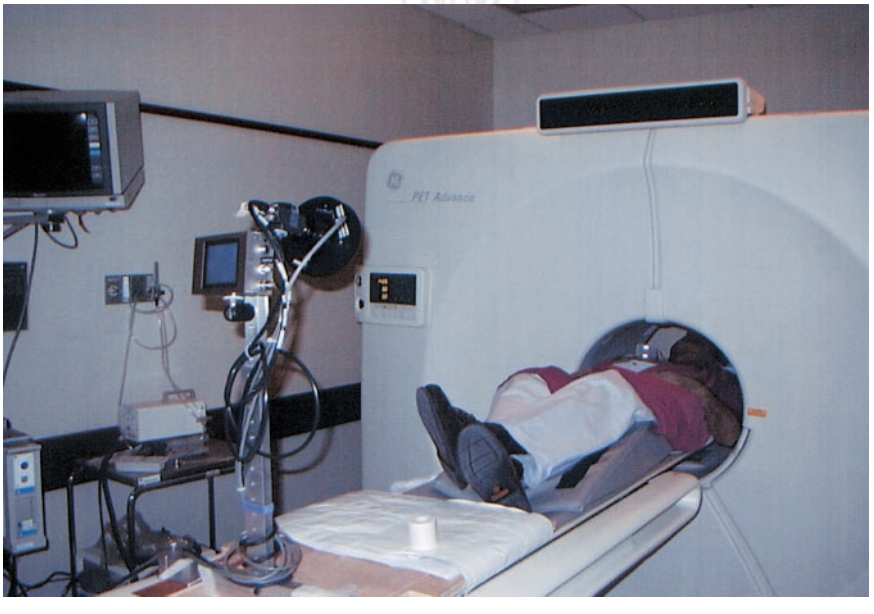

FIGURE 1. Patient setup in gated mode.

TABLE 1
Summary of Patients' Data

Patient no.	Sex	Age (y)	Tumor site	Tumor histology
1	F	59	Left hilum	NSCLC
2	F	83	Left lower lobe	NSCLC
3	F	40	Left peribronchial/ mediastinal	NSCLC
4	M	69	Right upper lobe	NSCLC
5	F	69	Left hilar	Squamous cell

NSCLC = non–small cell lung cancer.

ulation on an AcQSim (Picker International, Cleveland, OH). Patients were positioned supine with the arms up, using an Alpha Cradle (Alpha Cradle Molds, Akron, OH) to assist immobilization. The PET scans (static and gated) were obtained in the radiotherapy treatment position using the same immobilization technique. The least-moving areas (due to respiration) on the chest of the patient were chosen for the placement of 4 radioopaque markers on CT and PET scans. These areas were determined by observing the patient's respiration before obtaining the PET scan. The markers were used only to verify the integrity of the CT–PET registration but were not used to determine the registration.

Patients were injected intravenously with 370–555 MBq ^{18}F-FDG (provided by the Memorial Sloan-Kettering Cancer Center Radiochemistry/Cyclotron CORE facility) in sterile saline for injection, according to the United States Pharmacopeia standards. This was followed by an uptake phase with the patient in a recumbent position for approximately 45 min; the patient was then positioned in his or her mold on the PET table. The patient first underwent nongated whole-body PET 2-dimensional emission and transmission scanning for clinical management and treatment planning. The standard lung protocol at our center consists of 5 FOVs (14.25 cm per FOV). The total scan time is 35 min (7 min per FOV), consisting of a 4-min emission scan and a 3-min transmission scan. The gated PET study was then performed for just 1 bed position (at the lesion site), using the RPM system to track the motion of the gating block on the patient's chest. Just before image acquisition, the patient was coached to maintain relaxed breathing, and the RPM was used to ascertain the period of the breathing cycle used to determine the interval of the time bin. This study consisted of a 3-min transmission scan, a 10-min gated emission scan (10 bins), and a 3-min nongated emission scan for evaluation. The patient was coached continually during the gated phase to minimize any irregularity in the breathing cycle.

Analysis

The acquired PET data were reconstructed into (128 × 128) matrices using the ordered-subsets expected maximization (OSEM) algorithm, with segmented attenuation correction, and then corrected for attenuation, scatter, and randoms using software supplied by the manufacturer. The gating technique was then evaluated on the basis of the reduction in the total lesion volume measured in the gated mode compared with that in the nongated mode. The total lesion volume, measured in 1 bin, is the product of the slice thickness (4.25 mm) with the sum of the lesion cross sections, in all transaxial slices including the lesion, within the same time bin. The lesion cross sections were determined using the method of Erdi et al. (*7*). The upper gray scale threshold was set to the maximum activity concentration value within the lesion, whereas the lower threshold was set to 42% of the value of the upper level. This factor is determined on the basis of the signal-to-noise ratio in the PET images, as described in Erdi et al. The trigger is initialized on the basis of the regularity of the phase of breathing motion compared with that determined in the training session. Because of the irregularity in the patient's breathing cycle, only the first bin (corresponding to the trigger position) is reproducible. Consequently, only the data out of the first bin were considered for the gated study, on which the method of Erdi et al. was used to obtain the lesion region of interest. The effect of gating has been investigated on 2 semiquantitative parameters: the SUV, defined as the tissue concentration of ^{18}F-FDG in the structure delineated by the region of interest (kBq/mL) divided by the

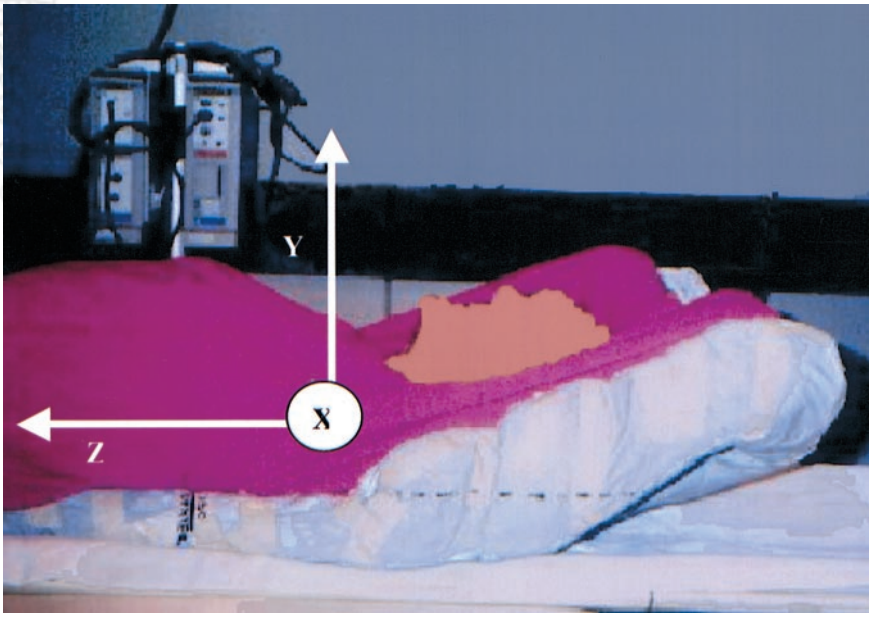

FIGURE 2. Patient coordinate system.

activity injected per gram of body weight (kBq/g); and the TLG, a parameter that measures the change in the total tumor glycolysis due to treatment. The TLG measure is defined as (*2*):

$$TLG = SUV \cdot Volume_{Lesion}. \quad \text{Eq. 1}$$

The effect of gating on the SUV and the TLG measurements was investigated through a comparison of the gated and the nongated modes for each of the 5 patients.

The relative motions of each lesion were estimated in *x*-, *y*-, and *z*-directions (Fig. 2). First, the centroid for each transaxial image (transaxial centroid) was calculated, weighting each pixel by its corresponding activity concentration. The centroid of the whole lesion volume was then calculated, weighting each transaxial centroid by the total activity concentration within the lesion in the corresponding transaxial slice. This was done on a bin-by-bin basis to calculate the motion amplitude determined by the maximum deviation of the centroid within the bins.

RESULTS

An example of the effect of gating on reducing the lesion size and shape is shown in Figure 3. This example shows a transaxial slice through 1 patient's lesion (patient 4) (Fig. 3A). This lesion shows a 13.7% reduction in the total lesion volume (Fig. 3B), which was accompanied by a 20.8% increase in the maximum SUV (SUV_{max}). The reduction in the tumor volume obtained by gating the ^{18}F-FDG PET scan allowed a decrease in the radiation therapy treatment volume (Fig. 3C). A comparison between the nongated and the gated modes of the measured lesion volumes for the 5 patients analyzed was performed (Fig. 4). Clinical results confirm phantom results (*5*) and show a reduction in the total lesion volume due to gating. This reduction in the smearing effect, by respiratory gating, leads to an increase in both SUV_{max} as a consequence of the shrinking in the apparent lesion volume (Fig. 5), as shown in the phantom studies (*5*). The percentage changes in the apparent lesion volumes and SUV_{max} are summarized in Table 2. In Figure 6, the maximum TLG (TLG_{max}) is estimated for the 5 patients in the nongated mode versus the gated mode. The data points are fit with linear functions, which show slopes of 1.01 and 0.97, respectively. Finally, Figure 7 shows the maximum lesion deviations in the lateral (*x*), anteroposterior (*y*), and superoinferior (*z*) directions for the 5 patients. The extremum amplitudes of the lesions' motions were 12.18 mm (patient 2) and 1.63 mm (patient 5), respectively, in the transaxial (*x*,*y*) plane. The variations in the *z*-direction are substantially smaller because 4 of the 5 lesions analyzed in this study were close to the apex of the lung.

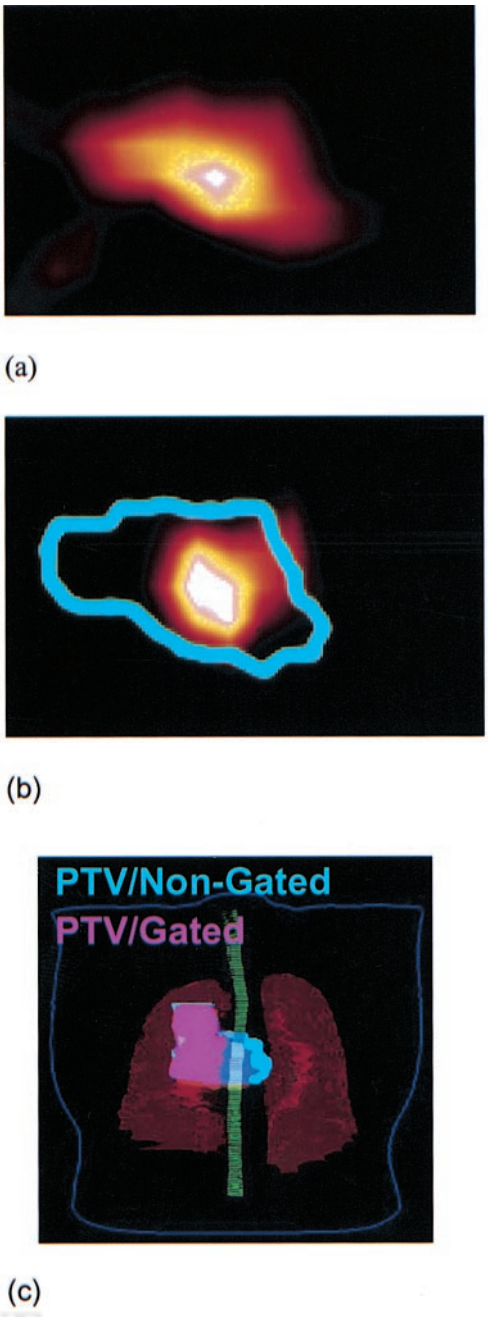

FIGURE 3. Transaxial ^{18}F-FDG PET image through 1 patient's lesion in nongated mode (A) and corresponding image in gated mode acquired in first bin (B). (C) Planning target volume in nongated (light blue) and gated (pink) modes. Note that light blue extends under whole pink area. Gating, in this particular case, has mainly spared left lung tissues from high doses.

DISCUSSION

This study reveals the capability to reduce the breathing motion artifacts by gating PET images in synchronization with respiration. The methodology was applied to 5 patients. A reduction in the apparent lesion volume ranging between 13.8% and 34.6% was achieved by gated acquisition relative to nongated acquisition. The magnitude of the reduction depends on the lesion size and motion amplitude as shown in phantom studies (*5*). This suggests that, in clinical applications, the effect of gating should depend on the lesion's size and site within the lung, which corresponds to different motion amplitudes.

The ability to gate PET scans will have a major impact on radiotherapy when the data are combined with gated or

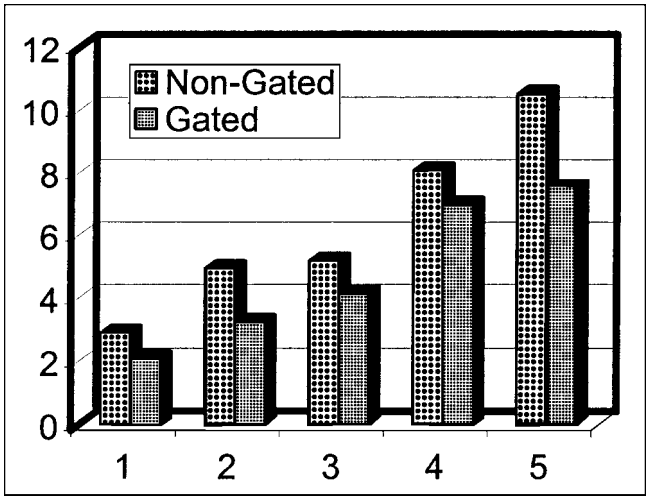

FIGURE 4. Comparison between lesion volumes in nongated and gated modes. Gating shows consistency in reducing apparent lesion volume.

deep-inspiration breath-hold CT. A more accurate, well-defined tumor will have 2 major consequences.

First, it will improve the definition of the tumor used for radiation treatment planning and, therefore, increase the sparing of normal tissues. This allows escalation of the dose within the tumor volume. So far, we have succeeded in integrating the gated images into the treatment planning system and registering them with nongated CT simulations. Future plans are to register the gated PET images with gated CT for a gated radiotherapy.

Second, as reported recently (*5*), this method will improve the quantitative accuracy of radiotracer uptake, which has been proven in phantom studies (*5*). We have analyzed the effect of gating on the measurements of SUV and TLG for ^{18}F-FDG. However, the method applies to any other tracer used to probe the biology of the tumor. This improved

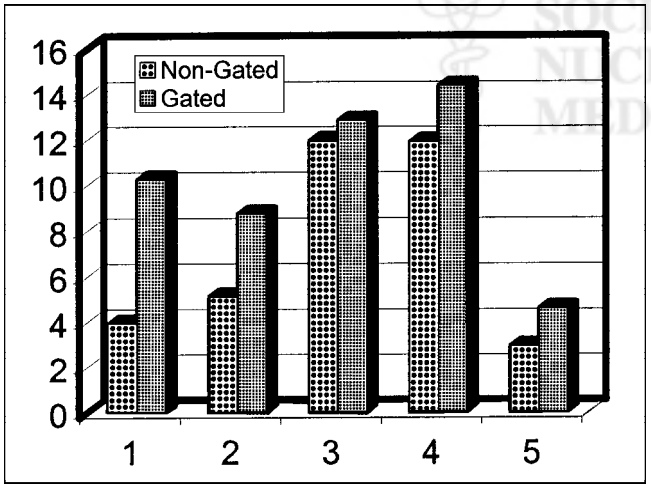

FIGURE 5. Comparison between SUV_{max} in nongated and gated modes. Gating shows consistency in improving accuracy in SUV_{max} measurements.

TABLE 2
Summary of Percentage Reduction in Lesion Volume and Percentage Increase in SUV_{max}

Patient no.	Volume (%)	SUV_{max} (%)
1	27.65633	159.1610
2	34.59119	70.4774
3	20.19324	7.4646
4	13.79567	20.8655
5	27.93120	56.5025

accuracy in quantitating the tumor can be very critical when it comes to monitoring its response to therapy. During the course of treatment, the patient's respiratory cycle might change because of many factors. As a consequence, the measured SUV might increase or decrease accordingly, even if the tumor remains stable. This may result in an incorrect evaluation of treatment response. SUV_{max} measurements for the 5 patients in this study showed an increase ranging from 7.46% to 156.16%. The most critical case was that of the first patient, for whom an increase in SUV_{max} from 3.95 to 10.25 was observed. Note that the reported SUVs in this study were measured using the iterative reconstruction with segmented attenuation-corrected (IRSAC) reconstruction algorithm. The SUV_{max} cutoff threshold is equal to 3.0 when measured with the IRSAC reconstruction algorithm. A measured SUV_{max} of 3.95 is close to the 3.0 cutoff threshold, which makes the confidence of any prediction of the lesion malignancy based on the SUV measurement less certain. However, a lesion with an SUV_{max} of 10.25 (in the gated mode) is less likely to be misqualified with false-positive findings. As mentioned earlier, the SUV cutoff threshold should be reconsidered for lung cancer when gating is used. On another hand, gating did not show any effect in the TLG measurements. As it was shown in Figure 6, TLG_{max} measurements are consistent in the 2 modes and showed a linear distribution with a slope of 1. This is expected because a reduction in the lesion volume is accompanied by an increase in the SUV_{max} by the same

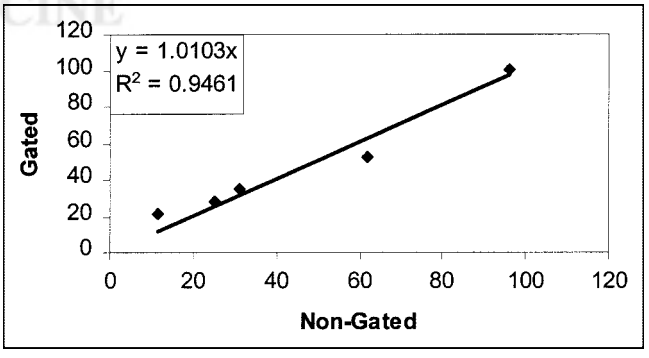

FIGURE 6. Maximum TLG (TLG_{max}) measurements in gated mode show linear dependence on those measured in nongated mode because increase in SUV_{max} should result in reduction in lesion volume by same factor.

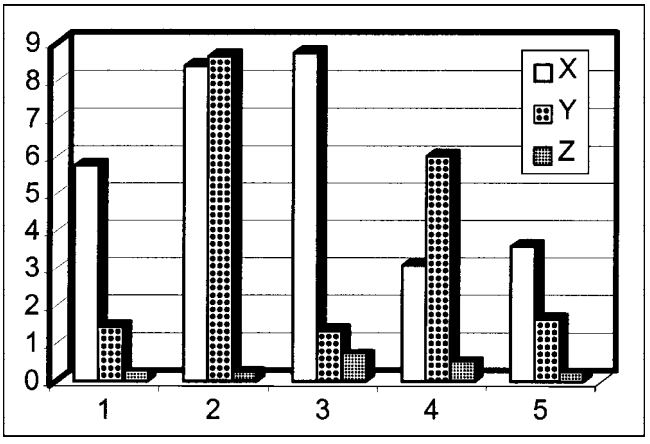

FIGURE 7. Maximum deviations of lesion centroids in *x*-, *y*-, and *z*-directions.

factor. This is true because the total activity concentration within the lesion is conserved.

Recent studies have shown that enhanced ^{18}F-FDG uptake in tumor is largely dependent on the elevated glucose metabolism. ^{18}F-FDG uptake is affected by tumor hypoxia (*8–10*), which is an important suspected reason for the failure of the radiotherapy (*11*) due to increased tumor radioresistance (*8*). The respiratory gating studies in this investigation will assist in improving the quantitation of regional tumor hypoxia with PET hypoxia imaging agents such as 1-^{18}F-fluoroalkyl-2-nitroimidazoles (*12*), ^{124}I-iodoazomycin-galactoside (*13*), and ^{64}Cu-labeled Cu(II)-diacetyl-bis(N^4-methylthiosemicarbazone (*14*). With dose sculpting using intensity-modulated radiation therapy, we can help to design a 3-dimensional dose map within the target volume, with appropriately weighted doses to voxels associated with acute hypoxia, which may not be possible with nongated methods due to signal smearing.

CONCLUSION

We have shown that respiratory motion can be a major effect in decreasing the accuracy in measuring the radiotracer uptake. A gating technique has been developed to account for respiratory motion artifacts in ^{18}F-FDG PET of lung cancer. Respiratory gating reduces activity smearing on PET images. Consequently, an improved accuracy in defining and quantitating the tumor, in particular through the SUV measurement, is observed. This method also offers the ability to more accurately monitor treatment response in lesions in the thorax.

ACKNOWLEDGMENTS

The authors thank all who have contributed to these promising results, in particular Dr. Hassan Mostafavi (Varian Medical Systems) for his help in integrating the RPM system into the gated PET, Dr. Charles Stearns (General Electric Medical Systems) for his cooperation, Saul Miodownik for his help in designing the gating circuit for the PET scanner, and the members of the Memorial Sloan-Kettering Cancer Center mechanical and electronics shops for their help in designing different components of the experimental gating system. This study was supported in part by National Institutes of Health grant P01-CA-59017.

REFERENCES

1. Gupta NC, Tamim WJ, Graeber GG, et al. Mediastinal lymph node sampling following positron emission tomography with fluorodeoxyglucose imaging in lung cancer staging. *Chest*. 2001;120:521–527.
2. Larson S, Erdi Y, Akhurst T, et al. Tumor treatment response based on visual and quantitative changes in global tumor glycolysis using PET-FDG imaging: the visual response score and the change in total lesion glycolysis. *Clin Positron Imaging*. 1999;2:159–171.
3. Lowe VJ, Fletcher JW, Gobar L, et al. Prospective investigation of positron emission tomography in lung nodules. *J Clin Oncol*. 1998;16:1075–1084.
4. Brink I, Reinhardt MJ, Hoegerle S, et al. Increased metabolic activity in the thymus gland studied with ^{18}F-FDG PET: age dependency and frequency after chemotherapy. *J Nucl Med*. 2001;42:591–595.
5. Nehmeh SA, Erdi YE, Rosenzweig KE, et al. Effect of respiratory gating on reducing lung motion artifacts in PET imaging of lung cancer. *Med Phys*. 2002; 29:336–371.
6. Kubo H, Len P, Minohara S, Mostafavi H. Breathing-synchronized radiotherapy program at the University of California Davis Cancer Center. *Med Phys*. 2000; 27:346–353.
7. Erdi Y, Mawlawi O, Larson S, et al. Segmentation of lung lesion volume by adaptive positron emission tomography image thresholding. *Cancer*. 1997;80: 2505–2509.
8. Ling CC, Humm J, Larson S, et al. Towards multidimensional radiotherapy (MD-CRT): biological imaging and biological conformality. *Int J Radiat Oncol Biol Phys*. 2000;47:551–560.
9. Clave AC, Brown RS, Wahl RL. Fluorodeoxyglucose uptake in human cancer cell lines is increased by hypoxia. *J Nucl Med*. 1995;36:1625–1632.
10. Burgman P, O'Donoghue A, Humm J, et al. Hypoxia-induced increase in FDG uptake in MCF7 cells. *J Nucl Med*. 2001;42:170–175.
11. Hockel M, Schlenger K, Mitze M, et al. Hypoxia and radiation response in human tumors. *Semin Radiat Oncol*. 1996;6:3–9.
12. Rasey JS, Koh WJ, Evans ML, et al. Quantifying regional hypoxia in human tumors with positron emission tomography of (^{18}F) fluoromisonidazole: a pretherapy study of 37 patients. *Int J Radiat Oncol Biol Phys*. 1996;36:417–428.
13. Chapman JD, Engelhardt EL, Stobbe CC, et al. Measuring hypoxia and predicting tumor radioresistance with nuclear medicine assays. *Radiother Oncol*. 1998;46: 229–237.
14. Lewis JS, Laforest R, Buettner TL, et al. Copper-64-diacetyl-bis(N^4-methylthiosemicarbazone): an agent for radiotherapy. *Proc Natl Acad Sci USA*. 2001;98: 1206–1211.